Frontiers of Materials Science

Electronic Supplementary Material

Suppressing molecular self-aggregation enables dense co-assembled monolayers for efficient methylamine-free wide-bandgap perovskite solar cells

Tianyi Chen[1]*, Shichen Song[2]*, Qinwu Zeng[1], Cheng Song[2], Mingqiang Gao[1], Xinghe Fan[1], Tiezhou Wu[1], Yumin Liu[2], and Shaofu Wang (✉)[1]

1 Hubei Key Laboratory for High-efficiency Utilization of Solar Energy and Operation Control of Energy Storage System, School of Electrical and Electronic Engineering, Hubei University of Technology, Wuhan 430068, China

2 Jiangxi Key Laboratory of Advanced Ceramic Materials, Energy Storage and Conversion Ceramic Materials Engineering Laboratory of Jiangxi Province, School of Energy Science and Engineering, Jingdezhen Ceramic University, Jingdezhen 333403, China

E-mail: shaofu_wang@whu.edu.cn

* T.C. and S.S. These authors contributed equally to this work.

To quantify the effective coverage of the self-assembled monolayers (SAMs) on the ITO or ITO/NiO_x, cyclic voltammetry (CV) was carried out in a standard three-electrode cell. A platinum plate and an Ag/AgCl electrode (3.0 mol·L^{-1} KCl) served as the counter and reference electrodes, respectively, while an ITO substrate with an active area of 15 mm × 10 mm was used as the working electrode. Prior to measurement, NiO_x/SAM or NiO_x/DC SAM were sequentially deposited on ITO working electrodes. All CV tests were performed in an argon-saturated 0.1 mol·L^{-1} tetrabutylammonium hexafluorophosphate solution dissolved in 1,2-dichlorobenzene (o-DCB), with the ferrocene redox couple employed as an internal reference. The areal density of the SAMs (Γ^*) was derived from the linear dependence of the anodic peak current on the voltage scan rate, as expressed by the following equation:

$$i_{p,o} = \frac{n^2F^2}{4RTN_A} A\,\Gamma^* v$$

where $i_{p,o}$ is the oxidative peak current, v is the voltage scan rate, Γ^* is the areal density, and A is the electrode area. In addition, F is the Faraday constant, R is the universal gas constant, N_A is the Avogadro constant, and T is the temperature.

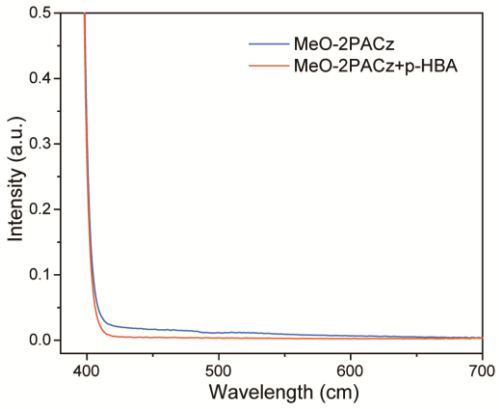


Fig. S1 UV–vis absorption spectra for MeO-2PACz and P-HBA/MeO-2PACz ethanol solutions.

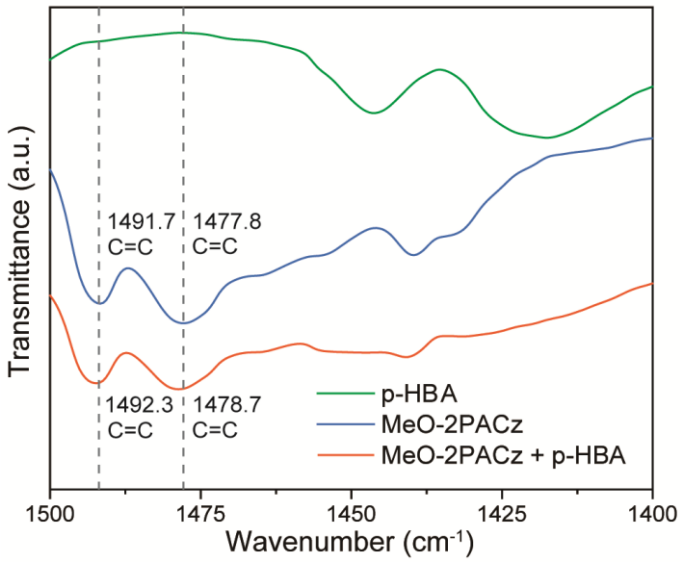


Fig. S2 FTIR spectra of MeO-2PACz, P-HBA, and MeO-2PACz/p-HBA mixture at 1500–1400 cm^{-1}.

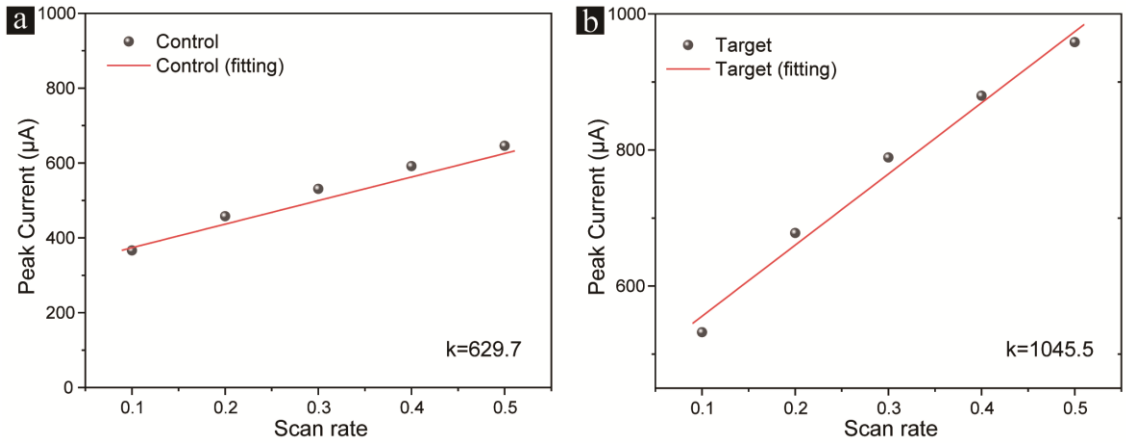


Fig. S3 The relationship between the oxidative peak current and the voltage scan rate for **(a)** Control HSC and **(b)** Target HSC.

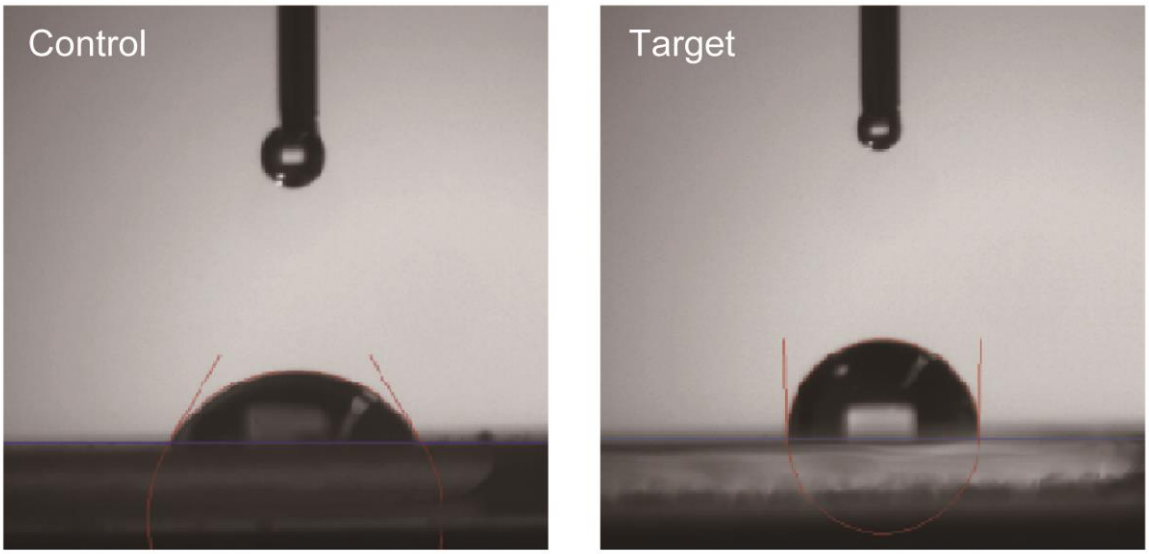


Fig. S4 Water contact angle images for Control and Target HSCs.

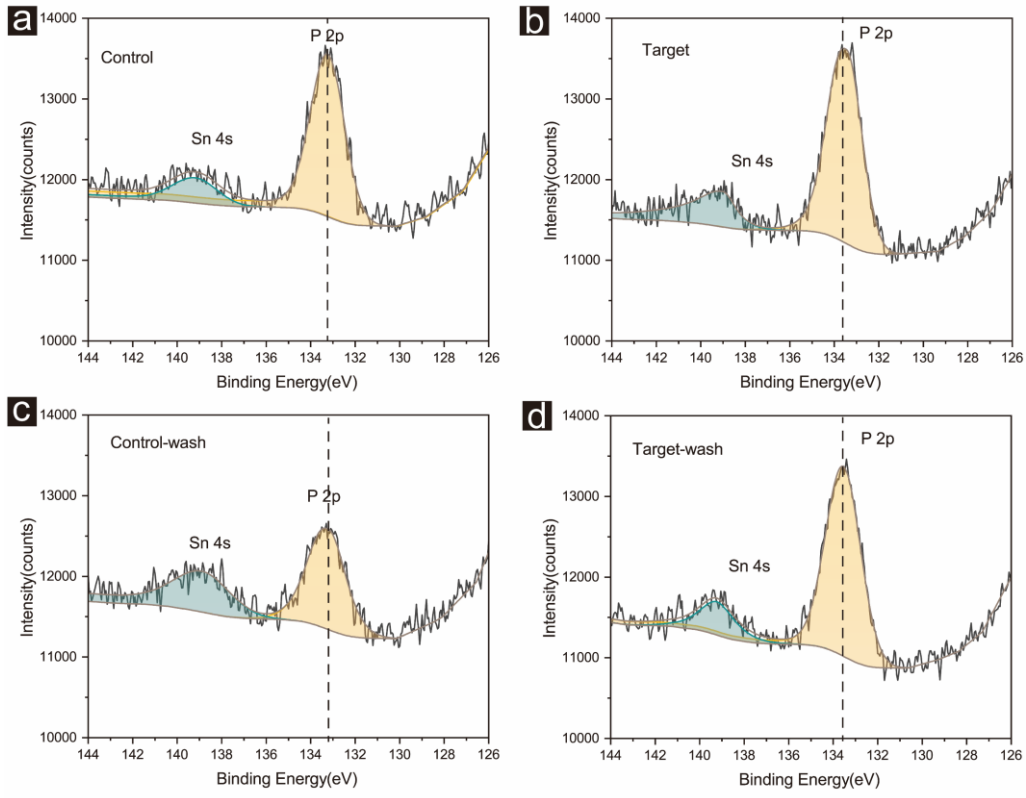


Fig. S5 XPS P 2p core-level spectra obtained for **(a)** Control HSC and **(b)** Target HSC without IPA washing, while **(c)** Control HSC and **(d)** Target HSC after IPA washing.

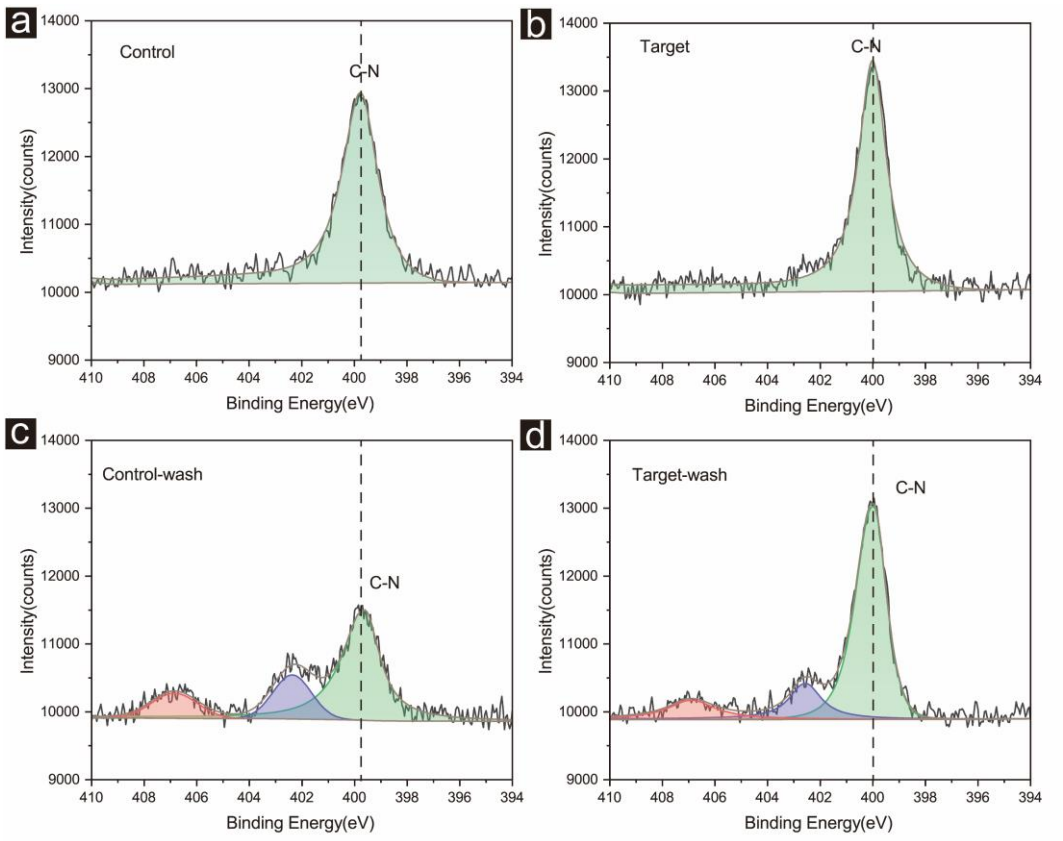


Fig. S6 XPS N 1s core-level spectra obtained for **(a)** Control HSC and **(b)** Target HSC without IPA washing, while **(c)** Control HSC and **(d)** Target HSC after IPA washing.

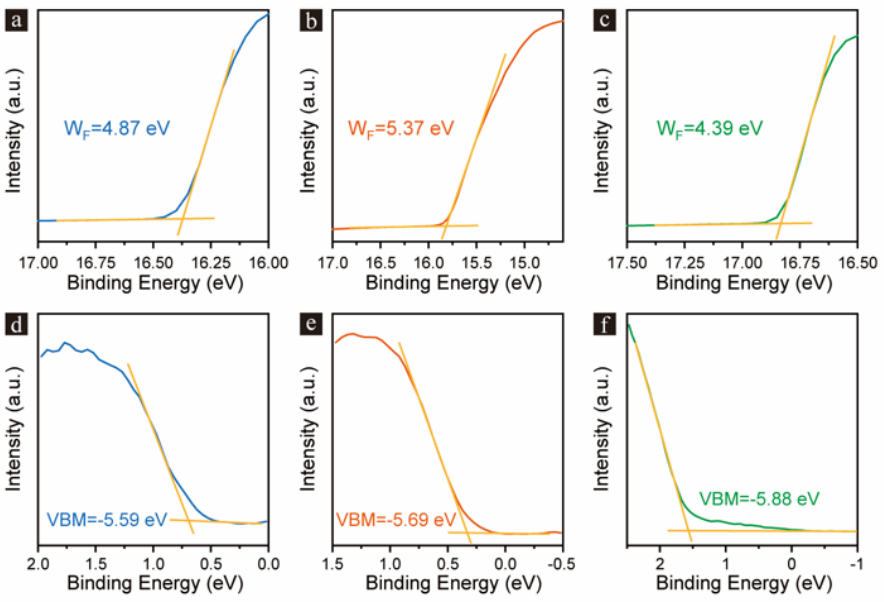


Fig. S7 Characteristics of the cutoff edge and Fermi edge in the UPS spectra of **(a)(d)** Control HSC, **(b)(e)** Target HSC, and **(c)(f)** WBG perovskite layer.

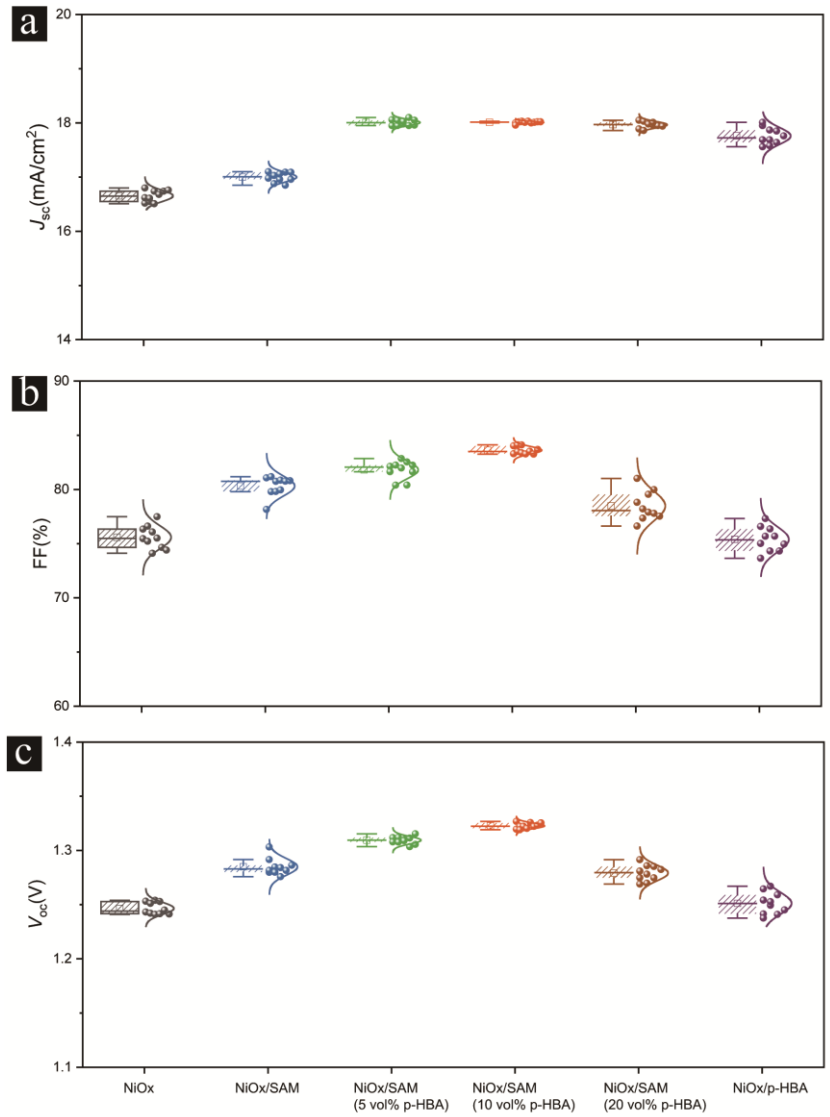


Fig. S8 Statistical distributions of **(a)** J_{sc}, **(b)** FF, and **(c)** V_{oc} for MA-free WBG PSCs based on different HSCs.

Table S1 Fitting parameters of TRPL decay spectra based on SAM and DC-SAM interfaces

Sample	τ_1/ns	A_1	τ_2/ns	A_2	τ_{ave}/ns
SAM	21.31	1320.13	121.124	422.62	85.72
DC-SAM	23.00	1047.17	134.42	525.95	106.41

The TRPL decay curve was fitted by using a double exponential decay:

$$y = y_0 + A_1\exp[-(x - x_0)/\tau_1] + A_2\exp[-(x - x_0)/\tau_2]$$

The average life time τ_{avg} can be calculated by:

$$\tau_{avg} = (A_1\tau_1^2 + A_2\tau_2^2)/(A_1\tau_1 + A_2\tau_2)$$

Table S2 The band structure parameters of different samples

Sample	W_S/eV	$(E_V - W_S)$/eV	E_V/eV
SAM	4.87	0.72	5.59
DC-SAM	5.37	0.32	5.69
PVK	4.39	1.51	5.90

Notes: W_S — the work function of the sample, which can be obtained by the cutoff edge from UPS measurements; $(E_V - W_S)$ — it can be obtained by the Fermi edge from UPS measurements; E_V — valence band edge.

Table S3 Fitting resistance parameters of different EIS measurements

Sample	R_s/Ω	R_{tr}/Ω	R_{re}/Ω
SAM	60.71	591.12	1010.34
DC-SAM	62.08	375.80	1904.00

The equivalent circuit diagram of Nyquist plots is shown as follows:

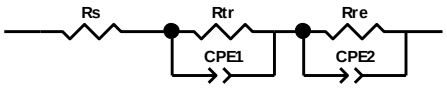


Table S4 Representative recent reports on wide-bandgap perovskite solar cells (1.75–1.80 eV) with SAM modification

Perovskite component	PCE/%	V_{oc}/V	E_g/eV	Ref.
$FA_{0.8}Cs_{0.2}PbI_{1.8}Br_{1.2}$	19.8	1.35	1.8	[S1]
$Cs_{0.2}FA_{0.8}Pb(I_{0.6}Br_{0.4})_3$	20.21	1.36	1.79	[S2]
$FA_{0.83}Cs_{0.17}Pb(I_{0.6}Br_{0.4})_3$	20.34	1.32	1.77	[S3]
$Cs_{0.2}FA_{0.8}Pb(I_{0.6}Br_{0.4})_3$	20.23	1.38	1.79	[S4]
$FA_{0.8}Cs_{0.2}PbI_{1.8}Br_{1.2}$	19.24	1.31	1.77	[S5]
$FA_{0.8}Cs_{0.2}Pb(I_{0.6}Br_{0.4})_3$	19.34	1.34	1.77	[S6]
$FA_{0.8}Cs_{0.2}Pb(I_{0.6}Br_{0.4})_3$	19.5	1.35	1.77	[S7]
$Cs_{0.2}FA_{0.8}PbI_{1.8}Br_{1.2}$	19.95	1.33	1.77	[S8]
$Cs_{0.4}FA_{0.6}Pb(I_{0.72}Br_{0.28})_3$	20.17	1.33	1.77	This work

References

[S1] Yi J, Bailey C, Leung T L, et al. Efficient ambient-all-laser-annealed wide bandgap perovskite solar cells. Advanced Functional Materials, 2025, 35(37): 2503971

[S2] Jia X, Zhang K, Gao X, et al. Defect passivation and crystallization modulation in methylammonium-free wide-bandgap perovskites for all-perovskite tandem solar cells. Science Advances, 2025, 11(38): eadv4501

[S3] Li H, Regaldo D, Wu C S, et al. Design of strong and weak intermolecular interactions to engineer buried interfaces in inverted wide-bandgap perovskite solar cells. Energy & Environmental Science, 2025, 18(13): 6618–6627

[S4] Chen M, Jiang W, Wang D, et al. Localized 2D/3D heterojunction enhances photovoltage for perovskite-organic tandem solar cells. Nature Communications, 2026, 17(1): 2093

[S5] Ma Z, Wu S, Yin X, et al. Bilayer hole-selective contact enhancing hole extraction for efficient inverted wide-bandgap perovskite solar cells. ACS Applied Materials & Interfaces, 2026, 18(19): 27519–27529

[S6] Wu Z, Zhao Y, Wang C, et al. Enhancing photovoltaically preferred orientation in wide-bandgap perovskite for efficient all-perovskite tandem solar cells. Advanced Materials, 2025, 37(8): 2412943

[S7] Li W, Liu G, Wen X, et al. Suppressing halide segregation of wide bandgap perovskite by interface molecular coordination for high-performance all-perovskite tandem solar cells. Angewandte Chemie International Edition, 2025, 64(44): e202511743

[S8] Zhong C, Wang J, Shi Z, et al. “Standing up” SAMs for efficient wide bandgap and all-perovskite tandem solar cells. Advanced Materials, 2026, 38(28): e202521898